ACS NANO
Cite This: ACS Nano 2018, 12, 298–307
www.acsnano.org

ARTICLE

Site-Selective Carving and Co-Deposition: Transformation of Ag Nanocubes into Concave Nanocrystals Encased by Au–Ag Alloy Frames

Jaewan Ahn, Daniel Wang, Yong Ding, Jiawei Zhang, and Dong Qin*

School of Materials Science and Engineering, Georgia Institute of Technology, Atlanta, Georgia 30332, United States

Supporting Information

ABSTRACT: We report a facile synthesis of Ag nanocubes with concave side faces and Au–Ag alloy frames, namely Ag@Au–Ag concave nanocrystals, by titrating $HAuCl_4$ solution into an aqueous mixture of Ag nanocubes, ascorbic acid (H_2Asc), NaOH, and cetyltrimethylammonium chloride (CTAC) at an initial pH of 11.6 under ambient conditions. Different from all previous studies involving poly(vinylpyrrolidine), the use of CTAC at a sufficiently high concentration plays an essential role in carving away Ag atoms from the side faces through galvanic replacement. Concurrent co-deposition of Au and Ag atoms *via* chemical reduction at orthogonal sites on the surface of Ag nanocubes leads to the generation of Ag@Au–Ag concave nanocrystals with well-defined and controllable structures. Specifically, in the presence of CTAC-derived Cl^- ions, the titrated $HAuCl_4$ is maintained in the $AuCl_4^-$ species, enabling its galvanic replacement with the Ag atoms located on the side faces of nanocubes. The released Ag^+ ions can be retained in the soluble form of $AgCl_2^-$ by complexing with the Cl^- ions. Both the $AuCl_4^-$ and $AgCl_2^-$ in the solution are then reduced by ascorbate monoanion, a product of the neutralization reaction between H_2Asc and NaOH, to Au and Ag atoms for their preferential co-deposition onto the edges and corners of the Ag nanocubes. Compared with Ag nanocubes, the Ag@Au–Ag concave nanocrystals exhibit much stronger SERS activity at an excitation of 785 nm, making it feasible to monitor the Au-catalyzed reduction of 4-nitrothiophenol by $NaBH_4$ *in situ*. When the Ag cores are removed, the concave nanocrystals evolve into Au–Ag nanoframes with controllable ridge thicknesses.

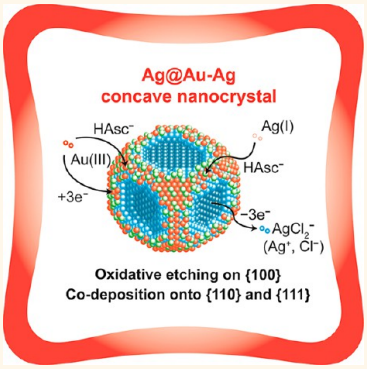

KEYWORDS: *bimetallic nanocrystals, concave nanocrystals, co-reduction, galvanic replacement, surface capping, surface-enhanced Raman scattering*

Noble-metal nanocrystals with concave structures on the surface are attractive for a range of applications in catalysis,[1,2] optical sensing,[3,4] and plasmonics.[5,6] Specifically, the high-index facets associated with a concave surface can be employed to enhance the catalytic activity by increasing the density of surface atoms with low-coordination numbers. The sharp features formed among or between concave faces can also lead to significant enhancement in local electric field, promoting their use as probes for surface-enhanced Raman scattering (SERS).[6−8]

There are two documented strategies for the synthesis of concave nanocrystals. The first one involves the use of an oxidative etchant to carve atoms from a specific set of facets on the nanocrystals for the creation of concave structures. Among those, Yang *et al.* demonstrated the fabrication of Ag concave nanocrystals by controlling the etching of Ag octahedra with a mixture of NH_4OH and H_2O_2.[9] Xia *et al.* reported the transformation of Pd nanocubes into Pd@Pt–Pd concave nanocubes by controlling the galvanic replacement reaction between Pd nanocubes and a Pt(II) precursor under the assistance of Br^- ions derived from KBr.[10] The second strategy relies on the selective deposition of atoms derived from a metal precursor at certain sites on the surface of a nanocrystal under the mediation of surface capping. To this end, Mirkin *et al.* demonstrated the fabrication of Au concave nanocubes and convex tetrahexahedra by varying the type of anions such as Cl^- and Br^- involved in the reaction.[11] Xia *et al.* reported the synthesis of Pt and Pd concave nanocubes by employing Br^- as a capping agent toward the {100} facets and thus slowing down the growth rate at these sites.[12,13] Xia *et al.* also demonstrated the deposition of Ag on Ag nanocubes for the generation of Ag concave nanocrystals by introducing Cu^{2+}

Received: September 6, 2017
Accepted: December 19, 2017
Published: December 19, 2017

DOI: 10.1021/acsnano.7b06353
ACS Nano 2018, 12, 298–307

ions into the solution to mediate the growth rates along different directions.[14] Huang *et al.* demonstrated the synthesis of Pd@Au concave nanocubes by introducing Ag^+ ions into the reaction solution under a reducing environment.[15] Wang *et al.* extensively explored the use of Cu^{2+} and Ag^+ ions in controlling the growth of Au nanorods into concave or convex Au nanorods with tunable aspect ratios.[16,17] Most recently, Personick *et al.* reported the use of I^- ions in manipulating the growth pattern of Pd on Au nanocrystals for the production of Au@Pd nanocrystals with a mix of concave and convex surfaces.[18]

Although the aforementioned approaches have been successfully implemented for the fabrication of nanocrystals with concave structures on the surface, few of these studies have explored the possibility to combine these two approaches together. We argue that the synergy of carving and deposition will offer some immediate advantages, including the ability to fabricate metal nanocrystals with more significant concaveness on the surface and the flexibility to manipulate the elemental compositions in addition to the spatial distributions of different elements. Herein, we demonstrate the synthesis of Ag nanocubes with concave side faces and Au–Ag alloy frames, namely Ag@Au–Ag concave nanocrystals, by titrating aqueous $HAuCl_4$ into an aqueous suspension of Ag nanocubes in the presence of ascorbic acid (H_2Asc), NaOH, and CTAC at an initial pH of 11.6. Distinctive from our prior work involving poly(vinylpyrrolidone) (PVP) for the generation of Ag@Au core–shell nanocubes[19,20] and Ag@Ag–Au core-frame nanocubes,[21] the use of CTAC sends the reaction along a different pathway for the transformation of Ag nanocubes into concave nanocrystals. Equivalent to PVP, CTAC can serve as a colloidal stabilizer to prevent the nanoparticles from aggregation in a colloidal suspension. However, the Cl^- ions dissociated from CTAC can affect both the speciation of the Au(III) precursor and the reduction/deposition pathway. Different from the PVP case, in which the galvanic replacement reaction was mainly inhibited by either the formation of $AuCl(OH)_3^-$ and $Au(OH)_4^-$ species under an alkaline condition[19] or the involvement of titrated Ag^+ ions under an acidic condition,[21] in the presence of Cl^- ions at a sufficient concentration, the added $HAuCl_4$ would be neutralized only by NaOH to form $AuCl_4^-$ species without further transformation into $AuCl(OH)_3^-$ and $Au(OH)_4^-$ species under an alkaline condition,[22] making it easier to initiate the galvanic reaction with Ag. Because the Cl^- ions have binding selectivity toward Ag(100) surface,[23] we argue that the dissolution of Ag atoms would occur on the side faces of Ag nanocubes. The released Ag^+ can be quickly converted to $AgCl_2^-$ by complexing with the Cl^- ions,[24] ruling out the formation of AgOH and then Ag_2O patches as it was observed in the case of PVP.[25] Under an alkaline condition, H_2Asc should be neutralized into ascorbic monoanion ($HAsc^-$),[26] a strong reducing agent, that can quickly reduce both $AuCl_4^-$ and $AgCl_2^-$ to Au and Ag atoms, respectively. When the side faces are dominated by the galvanic replacement reaction, the co-deposition of Au and Ag atoms should occur on the edges and corners of the nanocubes. As Ag atoms are continuously etched away from the side faces and more Au and Ag are codeposited on the edges and corners, the concavities on the side faces of the nanocubes are increasingly deepened toward the formation of Ag@Au–Ag concave nanocrystals. Such bimetallic nanocrystals embrace both the SERS activity arising from the original Ag cores and the catalytic capability through the introduction of Au to the surface, making them practical for monitoring Au-catalyzed reaction on the surface by *in situ* SERS. When the Ag cores are etched away selectively, the concave nanocrystals are transformed into Au–Ag alloy nanoframes with controllable ridge thicknesses. This study clearly demonstrates the feasibility to engineer the structures of bimetallic nanocrystals by manipulating the site selectivity of both etching and deposition through the introduction of a simple additive such as Cl^- ions.

RESULTS AND DISCUSSION

In a typical process, we followed an established protocol to prepare Ag nanocubes with an average edge length of 40.5 ± 2.8 nm (Figure S1).[27] We then dispersed the nanocubes in an aqueous solution containing H_2Asc, NaOH, and CTAC at an initial pH of 11.6, followed by the titration of 0.1 mM aqueous $HAuCl_4$ using a syringe pump under ambient conditions. Because the reaction solution was made alkaline by adding NaOH, essentially all the H_2Asc should be neutralized to generate $HAsc^-$, a much stronger reductant than H_2Asc.[26] Likewise, the titrated $HAuCl_4$ should be quickly neutralized by OH^- to form $AuCl_4^-$, which then potentially underwent ligand exchange with OH^- to produce $AuCl(OH)_3^-$ and $Au(OH)_4^-$, both of which have lower reduction potentials than $AuCl_4^-$.[22] However, the CTAC was supposed to dissociate into cetyltrimethylammonium (CTA^+) and chloride (Cl^-) ions in the reaction medium.[28] At an adequate concentration, we argue that the Cl^- ions should be able to keep the titrated Au(III) precursor in the form of $AuCl_4^-$ and thus maintain a relatively high reduction potential to support the galvanic replacement with the Ag nanocubes.

To validate our hypothesis, we performed two sets of experiments by titrating 0.1 mM $HAuCl_4$ into the aqueous suspension of Ag nanocubes in the presence of CTAC only. When NaOH was not involved in the reaction at an initial pH of 3.1, Figure S2A shows the UV–vis spectra of the Ag nanocubes before and after reacting with different volumes of $HAuCl_4$. It was found that the major LSPR peak of the Ag nanocubes was shifted from 433 to 468, 503, 499, and 523 nm at 0.2, 0.4, 0.6, and 0.8 mL, respectively, together with a continuing decrease in the peak intensity. Figure S2B shows transmission electron microscopy (TEM) image of the as-obtained sample prepared at a titration volume of 0.8 mL, in which voids were clearly identified. These results indicate the involvement of galvanic replacement reaction between Ag nanocubes and $HAuCl_4$ in the presence of CTAC and absence of NaOH.

When the initial pH of the reaction solution used in Figure S2A was 12.2 by adding the same amount of NaOH in the standard protocol, Figure S2C shows the corresponding UV–vis spectra of the Ag nanocubes at different titration volumes of $HAuCl_4$. Similar to the trend shown in Figure S2A, the major LSPR peak of the Ag nanocubes was shifted from 435 to 477, 548, 509, and 523 nm at 0.2, 0.4, 0.6, and 0.8 mL, respectively, together with some decrease in the peak intensity. Again, as shown in Figure S2D, we observed the formation of hollow interiors from the sample prepared at a titration volume of 0.8 mL. This observation is completely different from our previous observation in the presence of PVP rather than CTAC when all other reaction parameters were kept the same.[19,20] In the case of PVP under an alkaline condition, the galvanic replacement reaction between the Ag nanocubes and the added $HAuCl_4$ only occurred to a very minor extent. Taken together, under

DOI: 10.1021/acsnano.7b06353
ACS Nano 2018, 12, 298–307

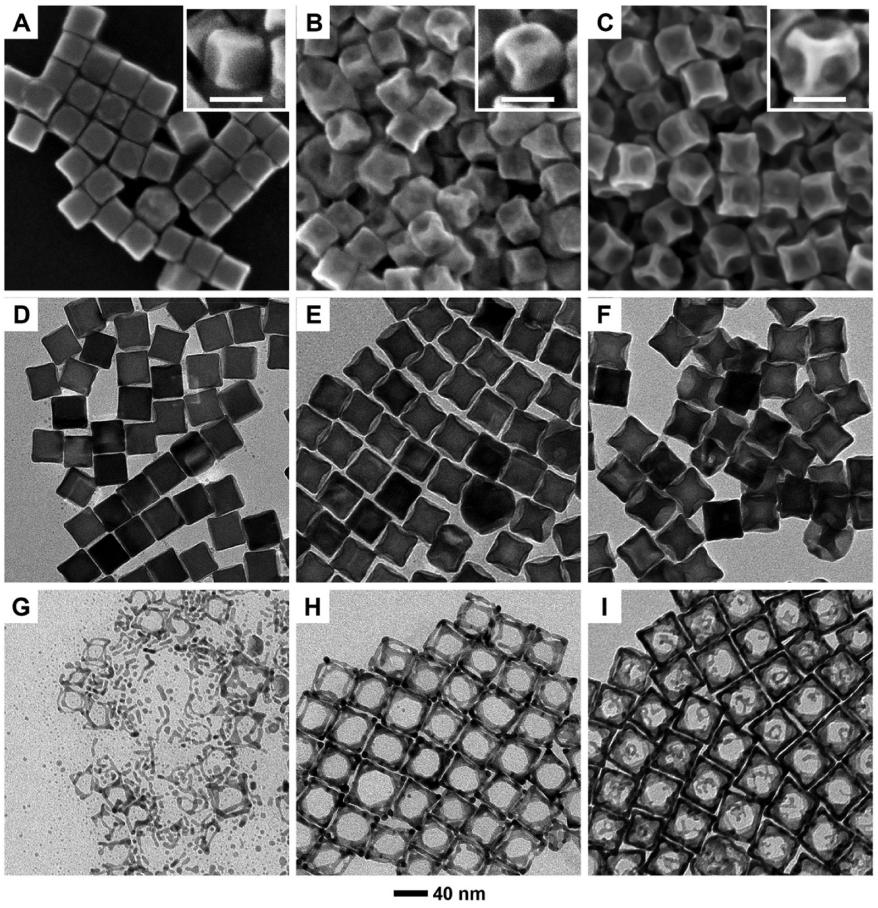

Figure 1. (A–C) SEM and (D–F) TEM images of the Ag@Au–Ag concave nanocrystals. The samples were prepared using the standard protocol by titrating different volumes of 0.1 mM aqueous $HAuCl_4$ into an aqueous suspension of Ag nanocubes in the presence of H_2Asc, NaOH, and CTAC at an initial pH of 11.6: (A, D) 0.2, (B, E) 0.8, and (C, F) 1.6 mL, respectively. (G–I) TEM images of the resultant structures after etching of the samples in (D–F) with aqueous H_2O_2. Scale bars in the insets: 40 nm.

the alkaline condition, we believe that the added $HAuCl_4$ was only neutralized by NaOH to generate $AuCl_4^-$ with no further ligand exchange with OH^-, enabling its galvanic replacement reaction with Ag nanocubes under the alkaline condition. The resultant Ag^+ ions remained in the soluble form of $AgCl_2^-$ by complexing with Cl^- ions.[24] Both the $AuCl_4^-$ and $AgCl_2^-$ in the reaction solution could be reduced by $HAsc^-$ to generate Ag and Au atoms for their co-deposition onto the Ag nanocubes.

Figure 1A–F shows scanning electron microscopy (SEM) and TEM images of the products obtained using the standard protocol, after adding different volumes of aqueous $HAuCl_4$. To help identify the Au deposition pathway, we used aqueous H_2O_2 to dissolve the Ag cores while leaving the deposited Au–Ag alloy intact. Figure 1G–I shows TEM images of the resultant structures. At a titration volume of 0.2 mL, Figure 1A,D shows nanoparticles with a similar morphology to that of the original Ag nanocubes, together with slightly sharpened corners. After the removal of Ag cores, Figure 1G shows the formation of broken nanoframes. In this case, the amount of Au atoms derived from the Au(III) precursor was insufficient to form continuous, robust structures on all the edges of the Ag nanocubes, leading to the formation of broken nanoframes. This result suggests that the initial deposition of Au selectively occurred on the edges, or the {110} facets, of Ag nanocubes, consistent with our previous findings.[21,29,30] When the titration volume was increased to 0.8 mL, Figure 1B,E shows the generation of nanocrystals with visibly concave side faces at the sites of {100} facets on the original Ag nanocubes. After the selective etching of Ag cores, Figure 1H confirms the transformation of the concave nanocrystals into cubic nanoframes as most of the Au atoms were deposited on the edges and then corners of the Ag nanocubes. As the titration volume was further increased to 1.6 mL, Figure 1C,F confirms the formation of cubic nanocrystals with more significantly concave side faces. After the removal of Ag cores, Figure 1I shows the creation of nanoframes made of ridges thicker than the sample shown in Figure 1H, while some Au atoms could also be found at the {100} facets. This observation suggests that some Au atoms could migrate from edges and corners to side faces through surface diffusion when a considerable amount of Au atoms are deposited on the nanocubes.[31]

We used aberration-corrected high-angle annular dark-field scanning TEM (HAADF-STEM) to examine the detailed structure and morphology of the as-obtained particles. We also performed energy dispersive X-ray spectroscopy (EDS) mapping on an individual particle to resolve the distributions of constituent elements. Figure 2A shows a HAADF-STEM image taken from an individual particle prepared using 0.8 mL of aqueous $HAuCl_4$, with the particle oriented along the ⟨001⟩ zone axis. We clearly observed the formation of concave side faces. Figure 2B–D shows the spatial distributions of Ag, Au, and Cl for the same nanocrystal shown in Figure 2A. We noticed that the distribution of Ag was confined to a solid

DOI: 10.1021/acsnano.7b06353
ACS Nano 2018, 12, 298–307

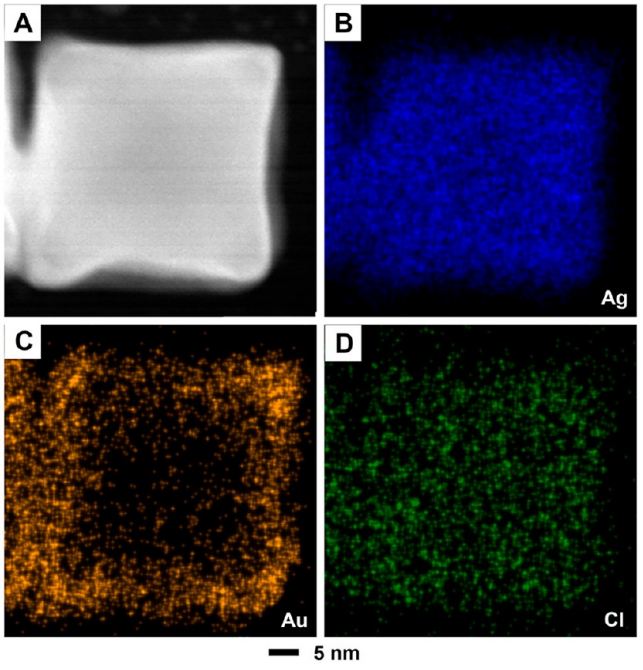

Figure 2. (A) HAADF-STEM image recorded from one of the Ag@Au−Ag concave nanocrystals prepared with a titration volume of 0.8 mL for $HAuCl_4$ (see Figure 1E), with the particle being orientated along the ⟨001⟩ zone axis. (B−D) EDS mapping of the same concave nanocube (blue: Ag; orange: Au; green: Cl).

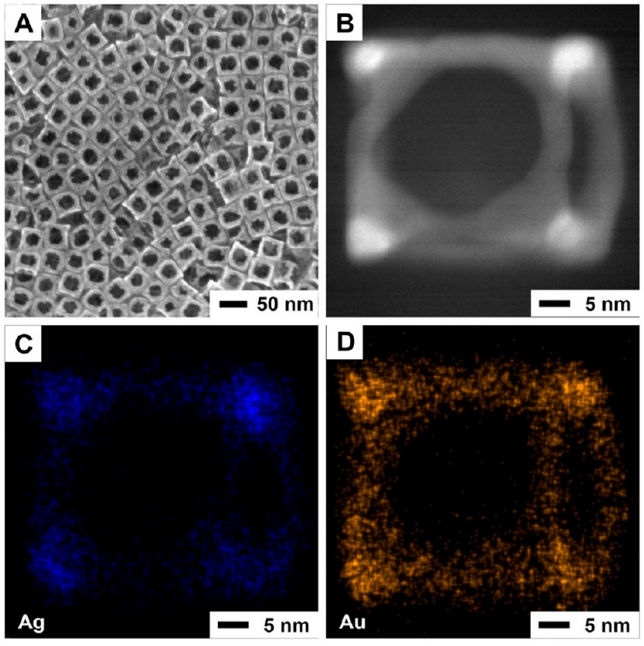

Figure 3. (A) SEM image of the nanoframes shown in Figure 1F. (B) HAADF-STEM image taken from one of the nanoframes shown in (A), with the particle being orientated along the ⟨001⟩ zone axis. (C, D) EDS mapping of a Au−Ag nanoframe (blue: Ag; orange: Au).

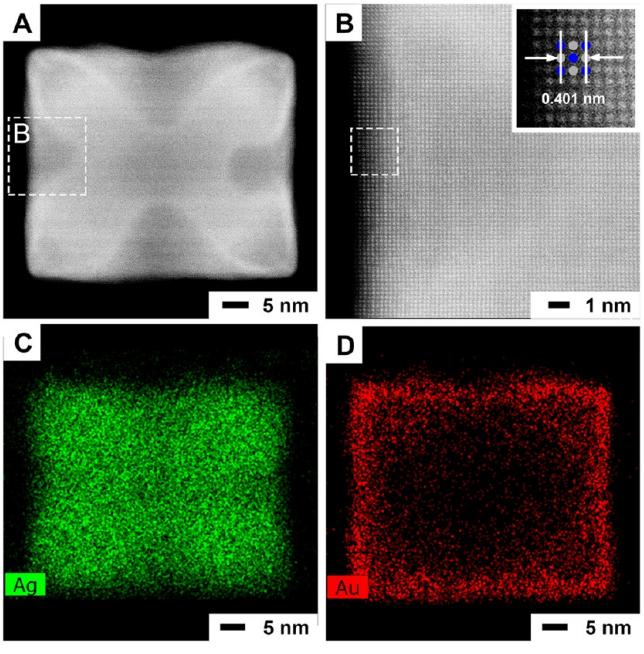

Figure 4. (A, B) HAADF-STEM images taken from one of the Ag@Au−Ag concave nanocrystal prepared with the titration of 1.6 mL of $HAuCl_4$ (see Figure 1F). The particle was orientated along the ⟨001⟩ zone axis. (C, D) EDS mapping of the concave nanocrystal (green: Ag; red: Au).

square with no inclusion of hollow interior and no extrusion from the corner sites, while Au was largely deposited around the nanocube. These results suggest that there was a limited galvanic replacement reaction between the Au(III) species and the Ag nanocubes, while the Au atoms derived from the reduction by both Ag and $HASc^-$ were preferentially deposited onto the edges and corners of the Ag nanocubes. The presence of Cl^- on the entire surface validates the selective capping of CTAC toward the {100} facets on the Ag nanocubes.

To further confirm the deposition pathway for Au, we also used aqueous H_2O_2 to remove Ag for the sample prepared with 0.8 mL of aqueous $HAuCl_4$ and then characterized the resultant nanostructures. Figure 3A shows an SEM image of the resultant nanoframes. Figure 3B gives a HAADF-STEM image of an individual nanoframe. The sharp bright contrast at the corners signifies local abundance of Au. Figure 3C,D shows the distributions of Ag and Au in the nanoframe. Again, we confirm the presence of Au on the edges and corners of the nanoframe. Because a small amount of Ag was observed at the corner sites after etching, we argue that the Ag atoms were included in the structure as a Au−Ag alloy, making it possible for them to survive the etching process. This result suggests that some Ag^+ ions were released from the {100} facets due to the galvanic replacement reaction with $AuCl_4^-$. These Ag^+ ions, likely in the form of $AgCl_2^-$ complex due to the presence of Cl^- ions at a relatively high concentration, could be reduced by $HAsc^-$ to produce Ag atoms, followed by their co-deposition with the Au atoms on the edges and corners of the Ag nanocubes.

We also performed HAADF-STEM and EDS analyses on one of the nanocrystals prepared with a larger titration volume of aqueous $HAuCl_4$ at 1.6 mL. Figure 4A shows a HAADF-STEM image when the particle was oriented along the ⟨001⟩ zone axis. Evidently, we observed the regions with a darker contrast on the side faces and in the center, indicating the loss of Ag from the side faces and thus formation of cavities at these sites. Figure 4B reveals the atoms that were located in the concave region. Based on the atom arrangement, we measured the lattice constant of the nanocrystal to be 0.401 nm, which is close to the lattice constants of both Au and Ag (0.408 and

DOI: 10.1021/acsnano.7b06353
ACS Nano 2018, 12, 298−307

0.409 nm, respectively).[32] This result indicates that there was no lattice distortion in the concave region. The distribution of Ag in Figure 4C is consistent with the contrast pattern shown in Figure 4A. Figure 4D confirms the deposition of Au mainly on the {110} and {111} facets of the Ag nanocube, with a limited amount on the {100} facets. These data directly support our TEM observation of the resultant nanostructures after the removal of Ag from the core (see Figure 1I). Taken together, it is clear that Ag atoms were oxidized and dissolved from the {100} facets of Ag nanocubes *via* galvanic replacement with $AuCl_4^-$ and the released Ag^+ ions subsequently complexed with the Cl^- ions to generate $AgCl_2^-$ until it was co-reduced with $AuCl_4^-$ by $HAsc^-$ for the generation of Ag and Au atoms.

To validate our hypothesis that the Ag atoms dissolved from the {100} facets of the Ag nanocubes were deposited back onto the edges and corners of nanocubes with Au atoms, we used inductively coupled plasma mass spectrometry (ICP-MS) to measure the contents of Ag and Au in the as-prepared samples when Ag nanocubes were reacted with different volumes of 0.1 mM $HAuCl_4$. In a typical process, we collected both solids and supernatants after centrifugation to separately determine their Ag and Au contents by ICP-MS analysis. Figure 5A shows that the amount of Ag in the solid samples did not change from the initial value of 184 μg as the titration volume of 0.1 mM $HAuCl_4$ was increased up to 1.6 mL. The Ag content in the supernatant was <0.1% of that in the solid at all the titration volumes, suggesting no loss of Ag from nanocubes during the titration process. This result supports our argument that the Ag atoms oxidized from the side faces of Ag nanocubes were reduced by $HAsc^-$ to generate Ag atoms for their redeposition onto the edges and corners of the nanocubes, increasing the concaveness on the {100} facets of the nanocubes. In comparison, Figure 5B indicates that the amount of Au in the solid samples linearly increased from 8.7 to 31.7 μg as the titration volume of $HAuCl_4$ was increased from 0.2 to 1.6 mL. It was found that the Au content in the supernatant was also below the detection limit in the course of titration. By assuming that the added $AuCl_4^-$ precursor was completely reduced to Au atoms by chemical reduction with $HAsc^-$ and through galvanic replacement with Ag nanocubes, and then deposited onto the Ag nanocubes, we calculated the amount of Au in the solids at different titration volumes (see solid line in Figure 5B), which are close to the experimental values. These results confirm that the added $AuCl_4^-$ was completely reduced into Au atoms, followed by their deposition onto the Ag nanocubes.

In addition to the characterization of the as-prepared products by electron microscopy, we used UV−vis spectroscopy to monitor the transformation of Ag nanocubes into Ag@Au−Ag nanocrystals by analyzing the localized surface plasmon resonance (LSPR) properties of the Ag nanocubes before and after reacting with aqueous $HAuCl_4$ in the presence of H_2Asc, NaOH, and CTAC at an initial pH of 11.6. As the titration volume was increased, Figure 6 shows that the major LSPR peak of the Ag nanocubes was constantly red-shifted from 435 to 455, 473, 499, and 530 nm at titration volumes of 0.2, 0.4, 0.8, and 1.6 mL, respectively. Additionally, the intensity of the major LSPR peak showed an initial decrease and then increase during the titration process. The red-shift of the LSPR peak could be attributed to the emergence of cavities on the side faces of the nanocrystals.[7] The initial decrease in peak intensity could be accounted by considering the dissolution of Ag atoms

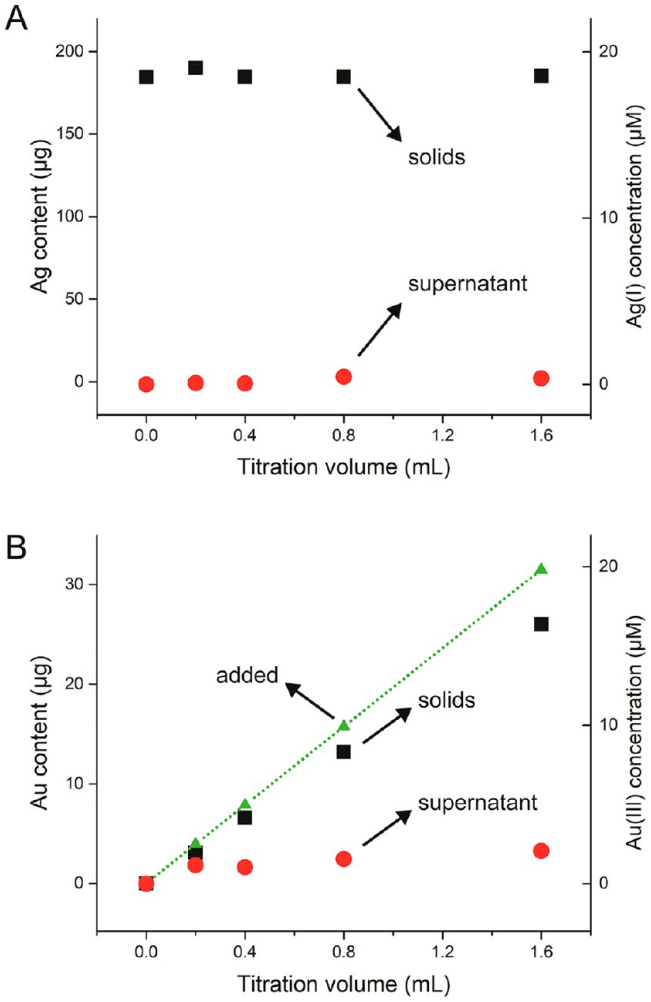

Figure 5. ICP-MS data of (A) Ag and (B) Au for the corresponding products (solids and supernatant) prepared using the standard protocol by titrating aqueous $HAuCl_4$ into an aqueous suspension of Ag nanocubes in the presence of H_2Asc, NaOH, and CTAC at an initial pH of 11.6. The data points marked as "added" represent the amount of Au calculated by assuming complete reduction for the added $HAuCl_4$, followed by the deposition of Au atoms onto the Ag nanocubes.

from the side faces and the deposition of Au on the edges and corners because Au has a weaker LSPR response in the visible region relative to Ag.[5] The subsequent increase in peak intensity could be ascribed to the reduction of the release Ag^+ ions for their co-deposition of the Au atoms.

To elucidate the explicit roles played by NaOH in transforming Ag nanocubes into the Ag@Au−Ag concave nanocrystals, we also recorded UV−vis spectra from Ag nanocubes before and after reacting with different volumes of 0.1 mM aqueous $HAuCl_4$ in the presence of H_2Asc and CTAC, but in the absence of NaOH at an initial pH of 2.8. Figure S3A shows the red-shift in LSPR peak position for the Ag nanocubes, together with broadening in peak width and a decrease in peak intensity. Figure S3B shows TEM image of the product obtained with a titration volume of 0.8 mL, from which we observed the transformation of Ag nanocubes into hollow nanocubes with slightly concave side faces. These results support our argument on the involvement of galvanic replacement reaction between Ag nanocubes and the Au(III) species in the presence of CTAC regardless of the initial pH.

DOI: 10.1021/acsnano.7b06353
ACS Nano 2018, 12, 298−307

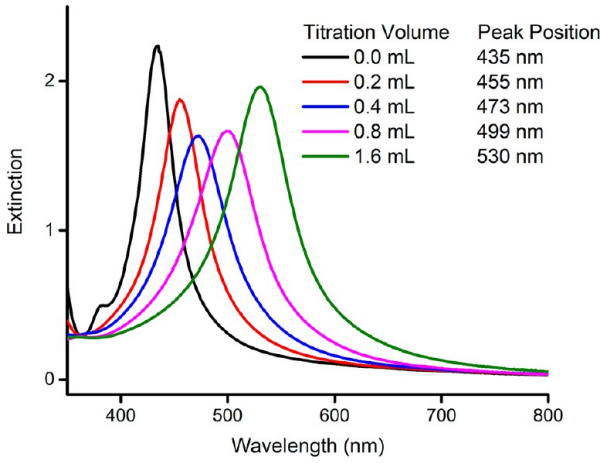

Figure 6. UV−vis spectra of Ag nanocubes before and after reacting with different volumes of 0.1 mM aqueous $HAuCl_4$ using the standard protocol in the presence of H_2Asc, NaOH, and CTAC at an initial pH of 11.6.

However, under an alkaline condition, NaOH would neutralize H_2Asc to $HAsc^-$, making the chemical reduction faster. Ultimately, the balance between galvanic reaction and chemical reduction would enable the generation of Ag concave nanocubes framed with a Au−Ag alloy at the corners and edges, different from the resultant structures produced in the absence of NaOH, or under an acid condition, when hollow interiors were created in the Ag nanocubes.

Based on the experimental results shown in Figures 1−6, we propose a mechanism to account for the transformation of Ag nanocubes into Ag@Au−Ag concave nanocrystals in an aqueous phase in the presence of H_2Asc, NaOH, and CTAC at an initial pH of 11.6 (Figure 7, left panel). Because the Cl^- ions derived from CTAC can selectively bind to the side faces, that is, {100} facets, on Ag nanocubes, we argue that these sites will be preferentially activated toward oxidation. Upon the titration of aqueous $HAuCl_4$, the {100} facets can act as an anode for the initiation of a galvanic replacement reaction between Ag and $AuCl_4^-$ species. The released Ag^+ ions should stay in the soluble form of $AgCl_2^-$ by complexing with Cl^- ions. Meanwhile, both the $AgCl_2^-$ and the Au(III) species can be reduced by $HAsc^-$ for the generation of Ag and Au atoms, followed by their deposition on the Ag nanocubes. Because the side faces are involved in the galvanic replacement reaction, we believe that the co-deposition of Au and Ag atoms is automatically directed and confined to the edges and corners. At a low titration volume of $HAuCl_4$, the site-selective deposition of Au and Ag atoms on the edges and corners is mainly responsible for the formation of slightly concave side faces when the carving on the side faces of nanocubes is limited. As more $HAuCl_4$ is titrated into the system, the Ag atoms are increasingly carved away from the side faces, leading to the formation of Ag@Au−Ag nanocrystals with more concaved side faces. Upon etching of pure Ag in the core with H_2O_2, the Ag@Au−Ag concave nanocrystals are transformed into Au−Ag nanoframes.

It is important to acknowledge that the deposition of Au on Ag nanocubes in the presence of CTAC is completely different from our previously published work in which PVP was used as the colloidal stabilizer, while all other experimental conditions were kept essentially the same (Figure 7, right panel).[20] In the case of PVP, the galvanic replacement reaction is initiated from the corner sites, the {111} facets, rather than the side faces due to insufficient Cl^- ions originating from the titrated $AuCl_4^-$ precursor to activate the {100} facets. The galvanic replacement is also quickly terminated due to the formation of AgOH and then Ag_2O patches at the corner sites. The formation of $AuCl(OH)_3^-$ and $Au(OH)_4^-$ through ligand exchange between $AuCl_4^-$ and OH^- also helps terminate the galvanic reaction by increasing the reduction potential of the Au(III) precursor. As a result, the titrated Au(III) precursor is mainly reduced by $HAsc^-$ to generate Au atoms, for their sequential deposition onto the edges and then side faces, leading to the transformation of Ag nanocubes into Ag@Au core−shell nanocubes. After the treatment with a weak acid to remove the Ag_2O and then etching of Ag cores with H_2O_2, the core−shell nanocubes are converted into Au-based nanoboxes with well-defined openings at the corners.[25]

We also investigated the role played by Cl^- ions in directing the deposition of Au and Ag on Ag nanocubes by replacing CTAC with NaCl as the source of Cl^- ions. We first tried to conduct the synthesis in the presence of NaCl instead of CTAC while keeping all other parameters the same as in the standard protocol. Without introducing PVP, however, the colloidal suspension became unstable upon the titration of $HAuCl_4$. As such, we had to add PVP to help stabilize the colloidal suspension. Specifically, we performed a set of experiments to monitor the transformation of Ag nanocubes by replacing the CTAC (0.1 M) with an equal volume of a mixture containing NaCl (0.1 M, the source of Cl^- ions) and PVP (1 mM, colloidal stabilizer). In this case, we titrated different volumes of 0.1 mM aqueous $HAuCl_4$ into a mixture containing Ag nanocubes, H_2Asc, NaOH, PVP, and NaCl at an initial pH of 11.4 (see details in the experimental session). Figure S4A shows that the major LSPR peak of the Ag nanocubes was red-shifted from 435 and 480 nm at titration volume of 0.8 mL, together a decrease in the peak intensity and some broadening in peak width. Upon etching the sample by 3% H_2O_2, we did not resolve any LSPR peaks. Figure S4B shows the TEM image of the product obtained after adding 0.8 mL of aqueous $HAuCl_4$, indicating a similar morphology to that of the original Ag nanocubes, except for the slightly sharpened corners. After removing the Ag in the core with H_2O_2, Figure S4C shows the formation of both nanoframes and nanoboxes. These results are completely different from those shown in Figures 6 and 1E,H, when CTAC was involved in the reaction solution in the absence of PVP. This result indicates that the presence of PVP could interfere the Cl^- ions, making the carving and deposition less site-selective. We have also attempted to perform a control experiment with CTAB instead of CTAC, but it was difficult to achieve the same concentration of 0.1 M due to its much lower CMC (0.001 M for CTAB vs 0.016 M for CTAC), making it impossible to obtain any meaningful results for direct comparison with those obtained from the use of CTAC

Collectively, CTAC at a sufficiently high concentration plays a number of roles in the transformation of Ag nanocubes into Ag@Au−Ag concave nanocrystals in an aqueous system. First, CTAC serves as a colloidal stabilizer to prevent the nanoparticles from aggregation in a colloidal suspension. Second, the CTAC-derived Cl^- ions would support the Au(III) species in the $AuCl_4^-$ form even under an alkaline condition, enabling the galvanic replacement reaction with the Ag nanocubes. Third, Cl^- ions can selectively bind to the {100} facets of Ag nanocubes, initiating the dissolution of Ag

DOI: 10.1021/acsnano.7b06353
ACS Nano 2018, 12, 298−307

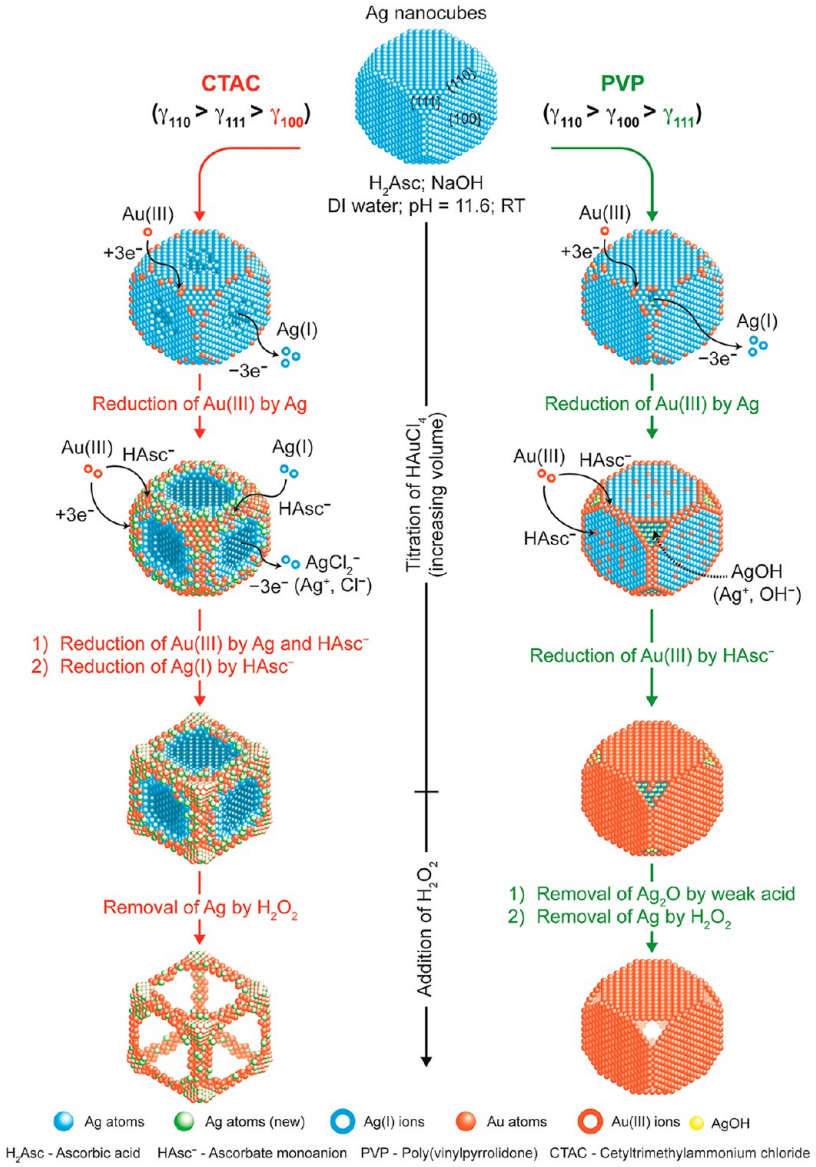

Figure 7. Schematic illustration describing the mechanisms proposed for the deposition of Au and Ag atoms on Ag nanocubes when $HAuCl_4$ is titrated into an aqueous suspension of Ag nanocubes in the presence of H_2Asc, NaOH, and CTAC (left) or PVP (right) at an initial pH of 11.6.

atoms from the side faces for the deposition of Au atoms on the edges and corners. Finally, the released Ag^+ ions from side faces of nanocubes can be retained in the soluble form of $AgCl_2^-$ by complexing with the Cl^- ions, and $AgCl_2^-$ can be reduced back to Ag atoms for their co-deposition with the Au atoms on the edges and corners of nanocubes.

We evaluated the SERS activity of Ag@Au−Ag concave nanocrystals by benchmarking against Ag nanocubes. With excitation at 785 nm, Figure S5 shows the SERS spectra collected from 4-nitrothiophenol (4-NTP) adsorbed on the Ag nanocubes and Ag@Au−Ag concave nanocrystals prepared with 1.6 mL of 0.1 mM aqueous $HAuCl_4$ (see Figure 1C). The SERS peak at 1574 cm^{-1} was increased 10 times for the concave nanocrystals (at 10% of laser power) relative to that of Ag nanocubes (at 100% laser power). The significant enhanced SERS activity could be attributed to the sharp features associated with the concavity of the Ag@Au−Ag nanocrystals.[33,34] We further demonstrated the use of these Ag@Au−Ag concave nanocrystals as a SERS probe for monitoring the reduction of 4-NTP by $NaBH_4$ *in situ* (Figure 8). In a typical measurement, we functionalized the concave nanocrystals with 4-NTP and then collected the SERS spectra at different time intervals after the introduction of $NaBH_4$ using the laser excitation wavelength at 785 nm. At t = 0 min, we observed the characteristic peaks of 4-NTP at 1111 cm^{-1} (C−N stretching mode, ν_{CN}), 1349 cm^{-1} (O−N−O stretching mode, ν_{NO_2}), and 1574 cm^{-1} (C−C stretching mode, ν_{CC}), respectively. The peak at 1083 cm^{-1} can be assigned to the C−S stretching mode (ν_{CS}). At t = 4 min, the three bands of 4-NTP remained essentially unchanged except that the ν_{NO2} band was slightly shifted from 1349 to 1336 cm^{-1}. At the same time, we began to resolve the characteristic peak of 4-ATP at 1593 cm^{-1} (C−C stretching mode, ν_{CC}), together with three emerging peaks associated with *trans*-dimercaptoazobenzene (*trans*-DMAB) at 1141 cm^{-1} (C−N stretching mode, ν_{CN}, and C−H bending mode, β_{CH}), 1390 cm^{-1}, and 1432 cm^{-1} (N═N stretching mode, ν_{NN}, C−N stretching mode, ν_{CN}, and C−H bending

DOI: 10.1021/acsnano.7b06353
ACS Nano 2018, 12, 298−307

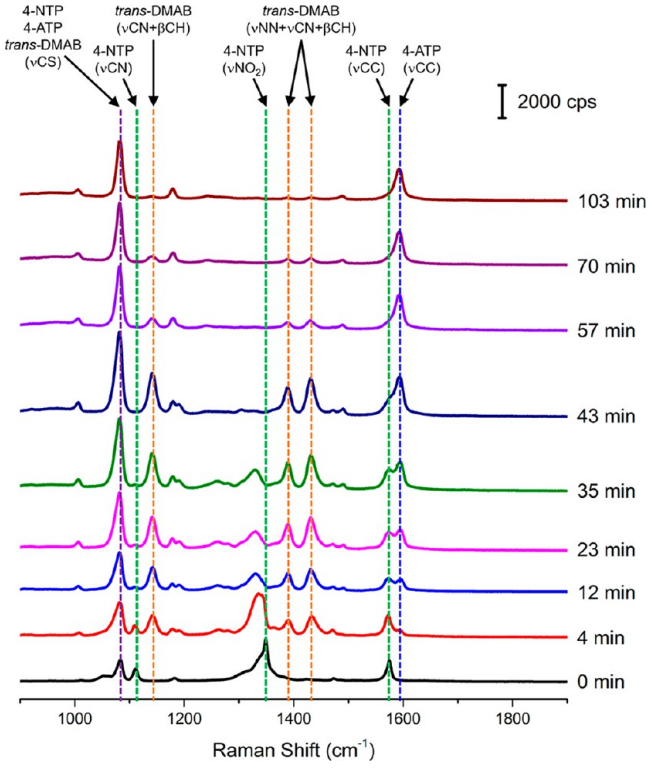

Figure 8. Time-dependent SERS spectra collected during the reduction of 4-NTP by $NaBH_4$ at an excitation wavelength of 785 nm. The reaction was catalyzed by the Ag@Au−Ag concave nanocrystals prepared using the standard protocol with the titration of 1.6 mL of 0.1 mM $HAuCl_4$.

mode, β_{CH}), respectively. As the reaction progressed to 12 and then 43 min, we observed the decrease in the peak intensities of three vibration bands for 4-NTP, while the peak intensities of the bands associated with 4-ATP and *trans*-DMAB were increased. At the reaction time of 57 min and beyond up to 103 min, the three peaks in the SERS spectra were assigned to 4-ATP, indicating the completion of reaction. These results suggest the reduction of 4-NTP to 4-ATP by $NaBH_4$ *via* the intermediate *trans*-DMAB, consistent with our previously published work.[34]

CONCLUSIONS

In summary, we have demonstrated the generation of Ag@Au−Ag concave nanocrystals by titrating aqueous $HAuCl_4$ into an aqueous suspension of Ag nanocubes in the presence of H_2Asc, NaOH, and CTAC at an initial pH of 11.6 under ambient conditions. Completely different from all the previous studies involving PVP, the use of CTAC sends the reaction along an unusual pathway. The mechanism involves the co-deposition of Au and Ag atoms on the edges and corners of the Ag nanocubes, while Ag atoms are concomitantly etched away from the side faces. Specifically, the added $HAuCl_4$ remains in the form of $AuCl_4^-$ under an alkaline condition, facilitating the galvanic replacement reaction with the Ag nanocubes. Because Cl^- ions can selectively bind to the {100} facets of Ag nanocubes, we argue that the dissolution of Ag atoms would occur from the side faces. The released Ag^+ ions could be retained in the soluble form of $AgCl_2^-$ by complexing with the Cl^- ions. Both the $AuCl_4^-$ and $AgCl_2^-$ are then reduced by $HAsc^-$ to generate Au and Ag atoms, followed by their preferentially co-deposition onto the edges and corners of Ag nanocubes. As the reaction progresses, Ag atoms located at the side faces of the nanocubes are continuously carved by the galvanic reaction, while Ag and Au atoms are increasingly deposited on the edges and corners, leading to the generation of Ag@Au−Ag nanocrystals with concave side faces. The concave nanocrystals show much stronger SERS activity at 785 nm excitation, making it feasible to monitor the Au-catalyzed reduction of 4-nitrothiophenol by $NaBH_4$ *in situ*. The concave nanocrystals could be transformed into Au−Ag nanoframes with controllable ridge thicknesses upon the removal of Ag in the core.

EXPERIMENTAL SECTION

Chemicals. Ethylene glycol (EG) was purchased from J. T. Baker. Silver trifluoroacetate (CF_3COOAg, 98%), gold(III) chloride trihydrate ($HAuCl_4{\cdot}3H_2O$, 99.9+%), sodium hydrosulfide hydrate ($NaHS{\cdot}xH_2O$), poly(vinylpyrrolidone) (PVP) with an average molecular weight of 29,000 (PVP-29), aqueous hydrochloric acid (HCl, 37 wt %), aqueous cetyltrimethylammonium chloride (CTAC, 25 wt %), L-ascorbic acid (H_2Asc, 99%), thiourea (99.0+%), acetone (99.5+%), sodium borohydride ($NaBH_4$, 99.99%), 4-nitrothiophenol (4-NTP, 80%), and aqueous hydrogen peroxide (H_2O_2, 30 wt %) were ordered from Sigma-Aldrich (St. Louis, MO). Sodium hydroxide (NaOH, 98%) was obtained from Alfa Aesar. All chemicals were used as received. All aqueous solutions were prepared using deionized (DI) water with a resistivity of 18.2 MΩ·cm at room temperature.

Synthesis of the Ag Nanocubes. We prepared the Ag nanocubes with an average edge length of 40.5 ± 2.8 nm using the polyol method developed by Xia and co-workers.[26] The as-obtained Ag nanocubes were washed with acetone and water once each and then dispersed in water for further use.

Synthesis of the Ag@Au−Ag Nanocrystals. In a standard protocol, 2 mL of aqueous CTAC (0.1 M) was added into a glass vial, followed by the addition of 0.5 mL of aqueous H_2Asc (0.1 M) and 0.5 mL of aqueous NaOH (0.2 M) under magnetic stirring. Immediately after the introduction of 25 μL of the aqueous suspension of Ag nanocubes (with a final concentration of about 2.6×10^{11} particles/mL), aqueous $HAuCl_4$ (0.1 mM) was titrated into the solution at a rate of 0.02 mL/min using a syringe pump under ambient conditions. As soon as the titration was completed, the solid sample was collected by centrifugation at 6000 rpm for 11 min, washed with water twice, and redispersed in water for future use. For the control experiment investigating the role of Cl^- ions, we replaced the 2 mL of aqueous CTAC (0.1 M) with a mixture of 1 mL of aqueous PVP (2 mM) and 1 mL of aqueous NaCl (200 mM) while keeping the other parameters the same in the standard protocol.

Etching of Ag Cores from the Ag@Au−Ag Nanocrystals. In a typical process, the as-prepared nanocrystals were dispersed in 0.1 mL of water, followed by the addition of 0.9 mL of aqueous H_2O_2 (3 wt %) solution. The suspension was left at room temperature for 5 h and then centrifuged at 12000 rpm for 15 min to collect the products. The particles were washed once with water and redispersed in water for further use.

Instrumentation and Characterization. The samples were washed and collected using an Eppendorf 5430 centrifuge (Eppendorf North America, Hauppauge, NY). The pH values were measured using a FiveEasy pH Meter (Mettler Toledo, Columbus, OH). The UV−vis spectra were collected using the Cary 60 spectrophotometer (Agilent Technologies, Santa Clara, CA). The Ag and Au contents in the nanocrystals were quantified using a NexION 300Q ICP-MS (PerkinElmer, Waltham, MA). TEM images were captured on a Hitachi HT7700 microscope (Tokyo, Japan) operated at 120 kV. SEM images were taken using a Hitachi SU8230 field-emission microscope. HAADF-STEM images were recorded on a Hitachi HD2700 C_s-corrected microscope operated at 200 kV. The EDS detector on the HD2700 was used to generate an elemental mapping of the nanocrystals.

DOI: 10.1021/acsnano.7b06353
ACS Nano 2018, 12, 298−307

SERS Monitoring of the Reduction of 4-NTP on the Ag@Au−Ag Nanocrystals. We first collected the as-prepared nanocrystals by centrifugation and had them dispersed in 0.1 mL of water. We then functionalized their surfaces with 4-NTP molecules by dispersing them in 0.9 mL of an ethanol-based 4-NTP solution (10^{-5} M). After incubation at room temperature for 2 h, we collected the 4-NTP-functionalized nanocrystals by centrifugation and washed with water prior to characterization. We took 0.2 mL of the suspension of 4-NTP-functionalized nanocrystals and mixed it with 0.2 mL of aqueous $NaBH_4$ (1 mg/mL) to start the reaction at room temperature. We sampled an aliquot of 20 μL from the reaction solution every several minutes and placed it in a polydimethylsiloxane (PDMS) sample cell to collect the SERS spectrum for monitoring the progress of the reaction. We used a Renishaw inVia Raman spectrometer (Wotton-under-Edge, UK) coupled with a Leica optical microscope (Leica Camera, Wetzlar, Germany) to collect the Raman spectra using 100× objective. We used an excitation wavelength of 785 nm in conjunction with a grating of 1200 lines/mm, and a maximum (100%) power of 100 mW. 10% of the maximum laser power was used to collect the Raman spectra from Ag@Au−Ag concave core-frame nanocubes as substrate, while 100% was used in the case of Ag nanocubes as substrate.

ASSOCIATED CONTENT

Supporting Information

The Supporting Information is available free of charge on the ACS Publications website at DOI: 10.1021/acsnano.7b06353.

Additional experimental details and data (PDF)

AUTHOR INFORMATION

Corresponding Author

*E-mail: dong.qin@mse.gatech.edu.

ORCID

Dong Qin: 0000-0001-5206-5912

Notes

The authors declare no competing financial interest.

ACKNOWLEDGMENTS

We acknowledge the support from the National Science Foundation (CHE-1412006), start-up funds from the Georgia Institute of Technology (GT), and a 3M nontenured faculty award. We acknowledge the use of the characterization facility at the Institute of Electronics and Nanotechnology (IEN) at GT.

REFERENCES

(1) Zhang, H.; Jin, M.; Xia, Y. Noble-Metal Nanocrystals with Concave Surfaces: Synthesis and Applications. *Angew. Chem., Int. Ed.* **2012**, *51*, 7656−7673.

(2) Burda, C.; Chen, X.; Narayanan, R.; El-Sayed, M. A. Chemistry and Properties of Nanocrystals of Different Shapes. *Chem. Rev. (Washington, DC, U. S.)* **2005**, *105*, 1025−1102.

(3) Willets, K. A.; Van Duyne, R. P. Localized Surface Plasmon Resonance Spectroscopy and Sensing. *Annu. Rev. Phys. Chem.* **2007**, *58*, 267−297.

(4) Jain, P. K.; Huang, X.; El-Sayed, I. H.; El-Sayed, M. A. Noble Metals on the Nanoscale: Optical and Photothermal Properties and Some Applications in Imaging, Sensing, Biology, and Medicine. *Acc. Chem. Res.* **2008**, *41*, 1578−1586.

(5) Haes, A. J.; Haynes, C. L.; McFarland, A. D.; Schatz, G. C.; Van Duyne, R. P.; Zou, S. Plasmonic Materials for Surface-Enhanced Sensing and Spectroscopy. *MRS Bull.* **2005**, *30*, 368−375.

(6) Rycenga, M.; Cobley, C. M.; Zeng, J.; Li, W.; Moran, C. H.; Zhang, Q.; Qin, D.; Xia, Y. Controlling the Synthesis and Assembly of Silver Nanostructures for Plasmonic Applications. *Chem. Rev. (Washington, DC, U. S.)* **2011**, *111*, 3669−3712.

(7) Xia, X.; Zeng, J.; McDearmon, B.; Zheng, Y.; Li, Q.; Xia, Y. Silver Nanocrystals with Concave Surfaces and Their Optical and Surface-Enhanced Raman Scattering Properties. *Angew. Chem., Int. Ed.* **2011**, *50*, 12542−12546.

(8) Rycenga, M.; Langille, M. R.; Personick, M. L.; Ozel, T.; Mirkin, C. A. Chemically Isolating Hot Spots on Concave Nanocubes. *Nano Lett.* **2012**, *12*, 6218−6222.

(9) Mulvihill, M. J.; Ling, X. Y.; Henzie, J.; Yang, P. Anisotropic Etching of Silver Nanoparticles for Plasmonic Structures Capable of Single-Particle SERS. *J. Am. Chem. Soc.* **2010**, *132*, 268−274.

(10) Zhang, H.; Jin, M.; Wang, J.; Li, W.; Camargo, P. H. C.; Kim, M. J.; Yang, D.; Xie, Z.; Xia, Y. Synthesis of Pd−Pt Bimetallic Nanocrystals with a Concave Structure through a Bromide-Induced Galvanic Replacement Reaction. *J. Am. Chem. Soc.* **2011**, *133*, 6078−6089.

(11) Zhang, J.; Langille, M. R.; Personick, M. L.; Zhang, K.; Li, S.; Mirkin, C. A. Concave Cubic Gold Nanocrystals with High-Index Facets. *J. Am. Chem. Soc.* **2010**, *132*, 14012−14014.

(12) Yu, T.; Kim, D. Y.; Zhang, H.; Xia, Y. Platinum Concave Nanocubes with High-Index Facets and Their Enhanced Activity for Oxygen Reduction Reaction. *Angew. Chem.* **2011**, *123*, 2825−2829.

(13) Jin, M.; Zhang, H.; Xie, Z.; Xia, Y. Palladium Concave Nanocubes with High-Index Facets and Their Enhanced Catalytic Properties. *Angew. Chem.* **2011**, *123*, 7996−8000.

(14) Xia, X.; Zeng, J.; Mcdearmon, B.; Zheng, Y.; Li, Q.; Xia, Y. Silver Nanocrystals with Concave Surfaces and Their Optical and Surface-Enhanced Raman Scattering Properties. *Angew. Chem.* **2011**, *123*, 12750−12754.

(15) Jiang, B.; Xu, L.; Chen, W.; Zou, C.; Yang, Y.; Fu, Y.; Huang, S. Ag-Assisted Heterogeneous Growth of Concave Pd@Au Nanocubes for Surface Enhanced Raman Scattering (SERS). *Nano Res.* **2017**, *10*, 3509−3521.

(16) Zhang, Q.; Zhou, Y.; Villarreal, E.; Lin, Y.; Zou, S.; Wang, H. Faceted Gold Nanorods: Nanocuboids, Convex Nanocuboids, and Concave Nanocuboids. *Nano Lett.* **2015**, *15*, 4161−4169.

(17) Zhang, Q.; Han, L.; Jing, H.; Blom, D. A.; Lin, Y.; Xin, H. L.; Wang, H. Facet Control of Gold Nanorods. *ACS Nano* **2016**, *10*, 2960−2974.

(18) King, M. E.; Personick, M. L. Bimetallic Nanoparticles: Bimetallic Nanoparticles with Exotic Facet Structures *via* Iodide-Assisted Reduction of Palladium. *Part. Part. Syst. Charact.* **2017**, *34*, 1600422.

(19) Yang, Y.; Liu, J.; Fu, Z.-W.; Qin, D. Galvanic Replacement-Free Deposition of Au on Ag for Core−Shell Nanocubes with Enhanced Chemical Stability and SERS Activity. *J. Am. Chem. Soc.* **2014**, *136*, 8153−8156.

(20) Sun, X.; Yang, Y.; Zhang, Z.; Qin, D. Mechanistic Roles of Hydroxide in Controlling the Deposition of Gold on Colloidal Silver Nanocrystals. *Chem. Mater.* **2017**, *29*, 4014−4021.

(21) Sun, X.; Qin, D. Co-titration of $AgNO_3$ and $HAuCl_4$: A New Route to the Synthesis of Ag@Ag-Au Core-Frame Nanocubes with Enhanced Plasmonic and Catalytic Properties. *J. Mater. Chem. C* **2015**, *3*, 11833−11841.

(22) Wang, S.; Qian, K.; Bi, X.; Huang, W. Influence of Speciation of Aqueous $HAuCl_4$ on the Synthesis, Structure, and Property of Au Colloids. *J. Phys. Chem. C* **2009**, *113*, 6505−6510.

(23) Zhou, S.; Li, J.; Gilroy, K. D.; Tao, J.; Zhu, C.; Yang, X.; Sun, X.; Xia, Y. Facile Synthesis of Silver Nanocubes with Sharp Corners and Edges in an Aqueous Solution. *ACS Nano* **2016**, *10*, 9861−9870.

(24) Du, J.; Chen, Z.; Chen, C.; Meyer, T. J. A Half-Reaction Alternative to Water Oxidation: Chloride Oxidation to Chlorine Catalyzed by Silver Ion. *J. Am. Chem. Soc.* **2015**, *137*, 3193−3196.

(25) Sun, X.; Kim, J.; Gilroy, K. D.; Liu, J.; König, T. A. F.; Qin, D. Gold-Based Cubic Nanoboxes with Well-Defined Openings at the Corners and Ultrathin Walls Less Than Two Nanometers Thick. *ACS Nano* **2016**, *10*, 8019−8025.

DOI: 10.1021/acsnano.7b06353
ACS Nano 2018, 12, 298−307

(26) Du, J.; Cullen, J. J.; Buettner, G. R. Ascorbic Acid: Chemistry, Biology, and the Treatment of Cancer. *Biochim. Biophys. Acta, Rev. Cancer* **2012**, *1826*, 443−457.
(27) Skrabalak, S. E.; Au, L.; Li, X.; Xia, Y. Facile Synthesis of Ag Nanocubes and Au Nanocages. *Nat. Protoc.* **2007**, *2*, 2182−2190.
(28) Wang, Z.; Larson, R. G. Molecular Dynamics Simulations of Thread like Cetyltrimethylammonium Choride Micllle: Effects of Sodium Choloride and Sodium Salicylate Salts. *J. Phys. Chem. B* **2009**, *113*, 13697−13710.
(29) Yang, Y.; Zhang, Q.; Fu, Z.-W.; Qin, D. Transformation of Ag Nanocubes into Ag−Au Hollow Nanostructures with Enriched Ag Contents to Improve SERS Activity and Chemical Stability. *ACS Appl. Mater. Interfaces* **2014**, *6*, 3750−3757.
(30) Wu, Y.; Sun, X.; Yang, Y.; Li, J.; Zhang, Y.; Qin, D. Enriching Silver Nanocrystals with a Second Noble Metal. *Acc. Chem. Res.* **2017**, *50*, 1774−1784.
(31) Xia, X.; Xie, S.; Liu, M.; Peng, H.-C.; Lu, N.; Wang, J.; Kim, M. J.; Xia, Y. On the Role of Surface Diffusion in Determining the Shape or Morphology of Noble-Metal Nanocrystals. *Proc. Natl. Acad. Sci. U. S. A.* **2013**, *110*, 6669−6673.
(32) Physical Constants of Organic Compounds. In *CRC Handbook of Chemistry and Physics*, 98th ed.; Rumble, J. R., Ed.; CRC Press: Boca Raton, FL, 2015.
(33) Hong, J. W.; Lee, S. U.; Lee, Y. W.; Han, S. W. Hexoctahedral Au Nanocrystals with High-Index Facets and Their Optical and Surface-Enhanced Raman Scattering Properties. *J. Am. Chem. Soc.* **2012**, *134*, 4565−4568.
(34) Zhang, J.; Winget, S. A.; Wu, Y.; Su, D.; Sun, X.; Xie, Z.-X.; Qin, D. Ag@Au Concave Cuboctahedra: A Unique Probe for Montioring Au-Catalyzed Reduction and Oxidation Reactions by Surface-Enhanced Raman Spectroscopy. *ACS Nano* **2016**, *10*, 2607−2616.

DOI: 10.1021/acsnano.7b06353
ACS Nano 2018, 12, 298−307